IOP Publishing Journal of Physics D: Applied Physics
J. Phys. D: Appl. Phys. **49** (2016) 025103 (7pp) doi:10.1088/0022-3727/49/2/025103

Effect of piezoelectric field on carrier dynamics in InGaN-based solar cells

Seunga Lee, Yoshio Honda and Hiroshi Amano

Department of Electrical Engineering and Computer Science, Graduate School of Engineering, Akasaki Research Center, Nagoya University, Chikusa-ku, Nagoya 464–8603, Japan

E-mail: seunga.lee@d.mbox.nagoya-u.ac.jp

Received 26 July 2015, revised 23 October 2015
Accepted for publication 30 October 2015
Published 30 November 2015

Abstract

To understand the effect of piezoelectric fields on carrier dynamics, we numerically investigated a simple p-GaN/i-$In_xGa_{1-x}N$/n-GaN solar cell structure. A reliable simulation model was obtained by comparing the experimental and simulated results in advance. The same p–i–n InGaN structures were re-simulated with and without the piezoelectric field effect, as spontaneous polarization remained unchanged. The sample with the piezoelectric field effect showed higher short current density (J_{sc}), a staircase-like feature in its I–V curve, and higher open circuit voltage (V_{oc}) with a lower fill factor (F.F.) and reduced conversion efficiency (C.E.) than the sample with no piezoelectric fields. In addition, with increasing In fraction (x), the V_{oc} value gradually increased while the J_{sc} value significantly decreased, correspondingly leading to a reduction in C.E. and F.F. values of the structure with the piezoelectric field effect. To solve the current loss problem, we applied various piezoelectric field elimination techniques to the simulated structures.

Keywords: photovoltaics, InGaN alloys, polarization effect, simulation

(Some figures may appear in colour only in the online journal)

1. Introduction

InGaN material systems have recently been recognized as high-efficiency photovoltaic (PV) systems because InGaN alloys have a direct band gap that covers nearly the entire solar spectrum by changing the indium (In) composition [1, 2]. According to an earlier theoretical calculation, InGaN alloys with approximately 40% In content can realize a highly efficient solar cell (SC) with a conversion efficiency (C.E) exceeding 50% [3]. Moreover, InGaN alloys exhibit various PV characteristics such as high carrier mobility, high radiation resistance, and high absorption coefficients that render them attractive candidates for SC applications [4, 5]. To channel these advantages into high-efficiency SCs, a thick high-quality InGaN layer with high In content is required. However for InGaN-based light-emitting diodes (LEDs) having similar structure with the SCs, it is well known that these requirements are difficult to achieve due to several factors causing degradation of device performance, such as high defect density [6, 7], severe In-segregation and existence of piezoelectric fields. In particular, piezoelectric fields are critical factors that hinder the growth of a high In contents InGaN layer because piezoelectric fields strengthen with increasing In content in the active region. Since the strong piezoelectric fields in general c-plane LEDs lead to decrease recombination efficiency by spatially separating the electron and hole wave functions in the active layer region [8], many researchers have extensively investigated ways of suppressing the piezoelectric fields. As in LEDs, the phenomenon responsible for the degradation of the device performance must be identified before the problem can be effectively solved. However, the correlation between the piezoelectric fields and carrier dynamics in InGaN-based SCs has not been reported to date, although the device mechanisms of SCs and LEDs are significantly different. Therefore, in this study, we numerically investigated the piezoelectric field effects on the carrier dynamics in InGaN-based p–i–n solar cells.

2. Simulation models and material parameters

The electro-optical properties of a simple p-GaN/i-$In_xGa_{1-x}N$/n-GaN solar cell structure were characterized by the simulation software SCSim under AM1.5 G, 1.5 sun illumination

Table 1. Material parameters of GaN and InN used in the simulations.

	GaN	InN
a (nm)	0.3188 [11]	0.3540 [12]
c (nm)	0.5186 [11]	0.5705 [12]
C_{11} (GPa)	374 [13]	223 [13]
C_{12} (GPa)	140 [14]	115 [13]
C_{13} (GPa)	106 [14]	94 [12]
C_{33} (GPa)	395 [15]	200 [12]
C_{44} (GPa)	101 [13]	46 [16]
e_{33} (C m^{-2})	0.65 [17]	0.43 [17]
e_{31} (C m^{-2})	−0.33 [17]	−0.22 [17]
e_{15} (C m^{-2})	−0.33 [17]	−0.22 [17]
P_{sp} (C m^{-2})	−0.029 [18]	−0.032 [18]

conditions. The simulation procedure of the software is detailed elsewhere [9]. Numerical analysis was implemented by calculating the light absorption, carrier generation rate, electron and hole transport statistics, and the electric potential from Poisson's equation in the 2D drift–diffusion model. Following Romanov *et al* [10], the numerical model also considered the total polarization induced by spontaneous and piezoelectric polarizations. In this process, the degree of piezoelectric fields was controlled by modifying not only the In fraction but also the strain relaxation constants (denoted ξ in the simulation). From the ξ values, the strained lattice constants of an arbitrary $In_xGa_{1-x}N$ compound layer are computed as follows:

$$a_R = (1 - \xi) \cdot a_S + \xi \cdot a_E(z) \quad (1)$$

$$c_R = (1 - \xi) \cdot c_S + \xi \cdot c_E(z), \quad (2)$$

where a_s and c_s are the lattice constants of the underlying layer, and a_E and c_E are the lattice constants of the free-standing compound layer, which vary along the z-axis (vertical to epitaxial layer) according to the material composition and the Vegard law, respectively. Thus, as ξ is increased, the piezoelectric polarization proportionally reduces while the spontaneous polarization remains unchanged. The piezoelectric polarization can be numerically eliminated when $\xi = 0$. The other relevant binary material parameters used in this study are listed in table 1.

For a robust investigation of the piezoelectric field effect, the investigated SC structure indicated in figure 1 was based on a c-plane free-standing GaN substrate with a dislocation density of 1×10^7 cm^{-2}. The p–i–n structure consisted of a 2000 nm thick Si-doped nGaN layer with a doping density of 4.5×10^{18} cm^{-3}, a 250 nm thick undoped $In_{0.1}Ga_{0.9}N$ absorption layer, and a 100 nm thick Mg-doped pGaN layer with a doping density of 3.6×10^{18} cm^{-3}. The device geometry was with a rectangular shape of 350×350 μm^2, which is similar to that of conventional GaN-based LEDs. The configuration and structural properties of this p–i–n SC structure were referred from the experimental study of Kuwahara *et al* [19].

3. Results and discussion

3.1. Confirming the reliability of simulation

To confirm the reliability of the simulation, the simulation results were compared with those of an experimentally

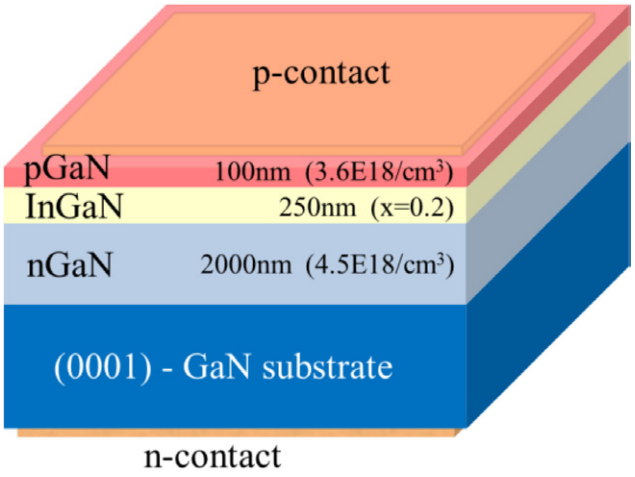

Figure 1. Schematic view of InGaN solar cell structure.

grown p–i–n InGaN SC with the same structural properties. Representative device performances and I–V characteristics for each case are presented in figure 2(a). As shown in the inset table of figure 2(a), the open circuit voltage (V_{oc}), short current density (J_{sc}), conversion efficiency (C.E.) and fill factor (F.F.) values of the simulated and experimental results were considerably similar. Besides the device performances, the shapes of the I–V curves were almost identical in the experimental and simulated results. In particular, both I–V curves exhibited a distinct staircase-like feature (the reason for this feature will be discussed in the next subsection). These comparisons confirm the reliability of our simulation model.

3.2. Effect of piezoelectric fields on carrier dynamics

Encouraged by the above results, we re-simulated the same p–i–n InGaN SC structure with a different strain relaxation constant ($\xi = 1$), thereby eliminating the piezoelectric fields in the structure, and observed the changes in carrier dynamics relative to the piezoelectric field case.

The simulated I–V curves and device performances of the p–i–n InGaN SC structures with and without piezoelectric fields are compared in figure 2(b). Observing these two cases, we confirm three notable differences between the structures with and without piezoelectric fields, namely the sample with piezoelectric fields showed increased V_{oc}, slightly increased J_{sc}, and staircase-like shape in the I–V curve. To understand these properties, the band diagram, recombination rate and carrier concentration plots for the structures with and without piezoelectric fields were obtained by priority under the zero bias voltage condition. The results are presented in figure 3. As revealed in the band diagrams, the energy band in the i-region of the structure with piezoelectric fields (figure 3(a)) was reversely tilted relative to that of the non-piezoelectric fields structure (figure 3(b)), due to the piezoelectric fields having opposite direction to built-in fields. Consequently as the incline angle of the energy band in the i-region was reduced in the structure with piezoelectric fields, predominant potential barriers were formed at each side of the InGaN/GaN interface. It was considered

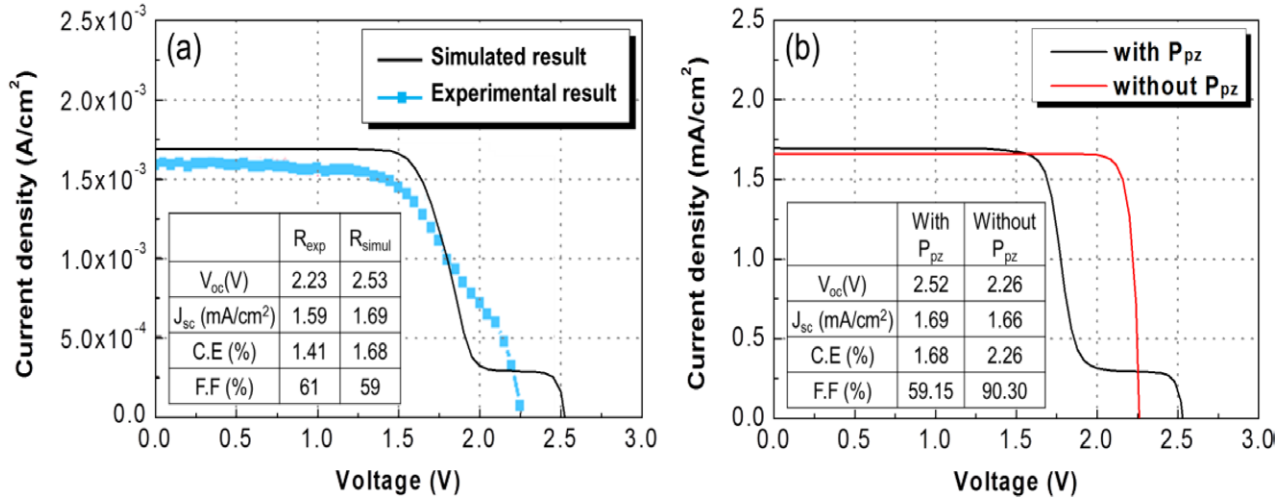

Figure 2. Comparison of the *I–V* characteristics of $In_{0.1}Ga_{0.9}N$ SC structures: (a) experimental and simulated results [19]; (b) structures with and without piezoelectric fields (P_{pz}).

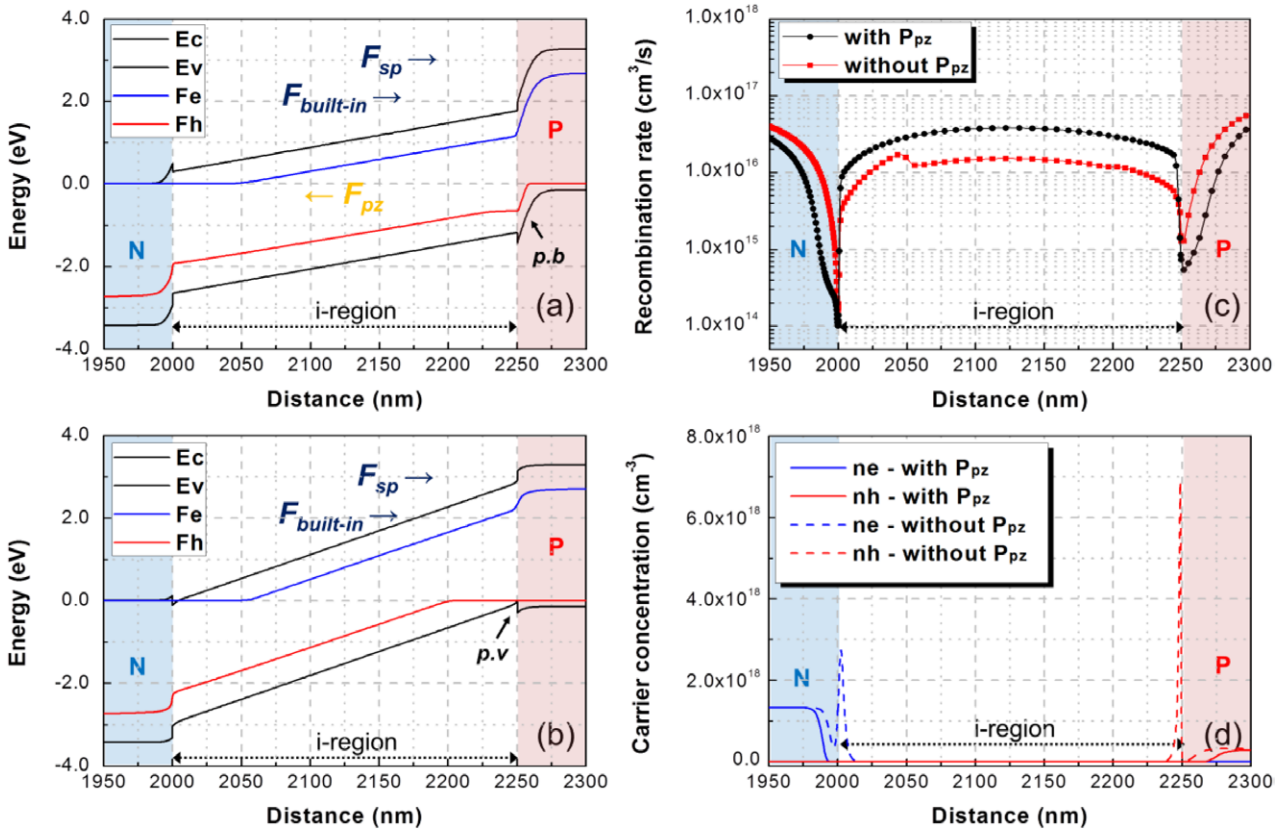

Figure 3. Various characteristics of the $In_{0.1}Ga_{0.9}N$ SC structure with and without piezoelectric fields (P_{pz}) at 0 V: (a), (b) band diagrams under different P_{pz} conditions, (c) recombination rates, and (d) carrier concentration plots.

that these predominant potential barriers, which are probably associated with drift and diffusion forces, greatly affect the V_{oc} property, in that the V_{oc} is determined by the bias voltage at which the drift force equals the diffusion force. As shown in figure 3(a), high predominant potential barriers at the interface region hinder the movement of diffused carriers, because the carriers require more energy to cross the barriers, although the drift force was negligibly reduced by increasing the bias voltage. Therefore, the drift and diffusion forces in the structure with piezoelectric fields became equalized at higher bias voltage, raising the V_{oc} relative to the structure without piezoelectric fields.

To investigate the J_{sc} property, the recombination rate and accumulated carrier concentration, which dominantly hinder carrier collection in the epitaxial field, were characterized in the i-region. Figures 3(c) and (d) indicated the recombination rate and carrier concentration, respectively, under the zero bias voltage condition that determines the J_{sc} value. The structure with piezoelectric fields manifested a higher recombination rate in the i-region than the structure without piezoelectric

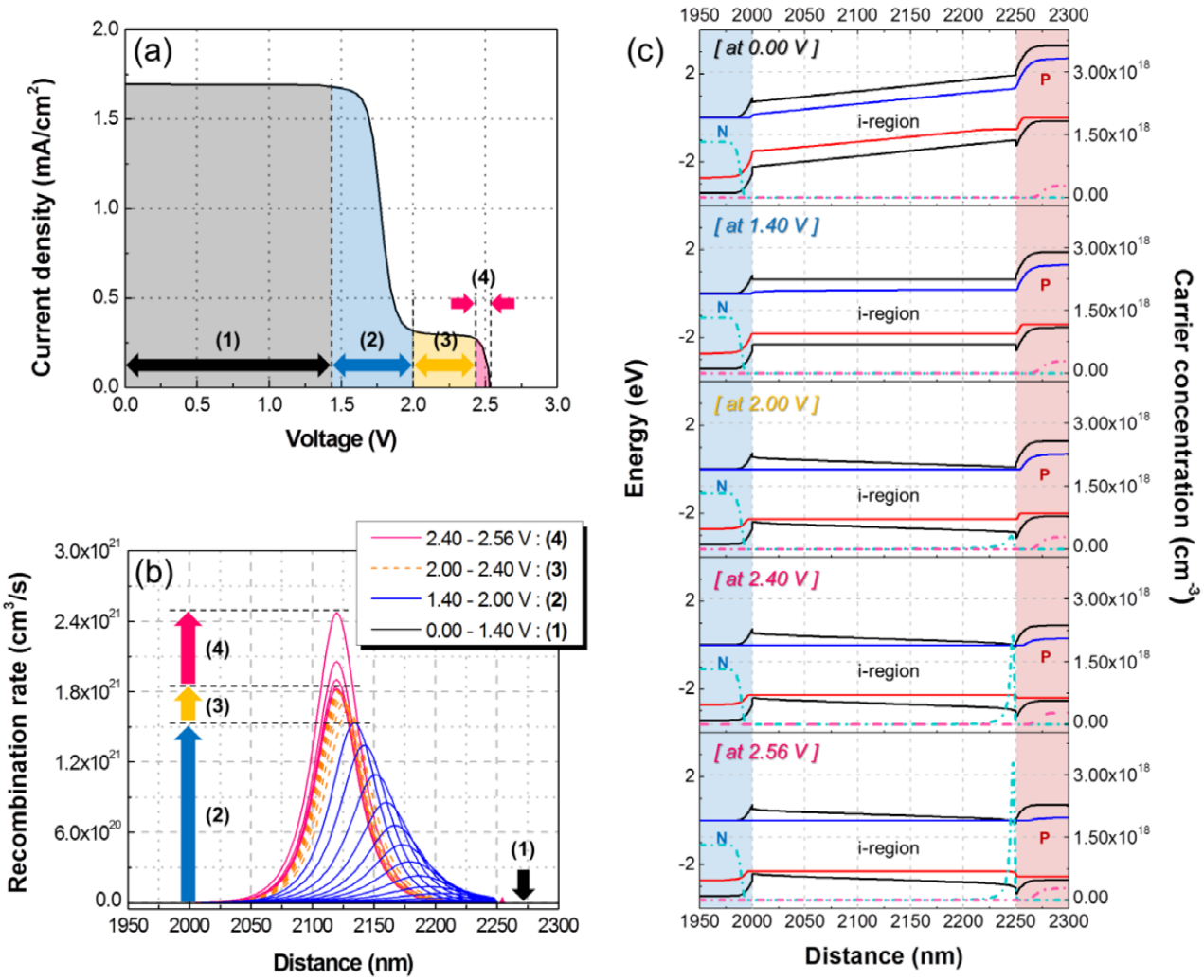

Figure 4. (a) *I–V* curves and (b) recombination rates in a $In_{0.1}Ga_{0.9}N$ SC structure with piezoelectric fields (P_{pz}) under different applied bias voltages (ranges 0–1.40 V (1), 1.4–2.0 V (2), 2.0–2.40 V (3), and 2.40–2.56 V (4)). (c) shows the corresponding band diagrams and carrier concentrations at specific applied bias voltages (solid and dotted lines indicate the energy band and carrier concentration, respectively).

fields (the maximum recombination rates in the structures with and without piezoelectric fields were 3.79×10^{16} cm^{-3} s^{-1} and 1.71×10^{16} cm^{-3} s^{-1}, respectively). This occurred because the angle of the energy band in the i-region was reduced in the structure with piezoelectric fields (figure 3(a)), suppressing the drift force and thereby promoting recombination of the photogenerated carriers in this region. However, this behaviour is contradicted by the spatial carrier distribution characteristic in terms of J_{sc} property. In figure 3(b), we observe that eliminating the piezoelectric fields significantly decreased the height of the potential barriers in the InGaN/GaN interface region, which is equivalent to potential valley formation in the interface regions. Moreover, the minimum states of the conduction and valence bands contacted their electron and hole Fermi levels, respectively. Because of these energy band shapes, numerous carriers accumulated at both n- and p-sides of the InGaN/GaN interface regions in the structure without piezoelectric fields. In contrast, negligibly few carriers accumulated in the same regions of the structure with piezoelectric fields (the maximum accumulated electron and hole concentrations were 5.16×10^{8} cm$^{-3,}$ and 2.26×10^{11} cm^{-3} respectively in the structure with piezoelectric fields, and 2.73×10^{18} cm^{-3} and 8.8×10^{18} cm^{-3} respectively in the structure without piezoelectric fields). Since J_{sc} is determined by the joint effects of recombination and spatial carrier distribution, it was slightly higher in the structure with piezoelectric fields than in the structure without piezoelectric fields. The underlying reason is accumulated carrier concentration in i-region for the structure without piezoelectric fields was extremely larger than increased amount of recombination rate in i-region for the structure with piezoelectric fields relatively.

To investigate the staircase-like feature of the *I–V* curve, we plotted the *I–V* characteristics and recombination rate in the i-region of the structure with piezoelectric fields. The plots are presented in figures 4(a) and (b), respectively. Comparing these two panels, we observed that in the 0–1.4 V and the 2.0–2.4 V ranges (labelled (1) and (3), respectively, in figure 4), the current density was almost constant in the *I–V* curve and the recombination rate in the i-region marginally increased. In contrast, in the 1.4–2.0 V and 2.4–2.54 V ranges (labelled (2) and (4), respectively, in figure 4), the current density was significantly decreased in the *I–V* curve by increasing the

bias voltage and the recombination rate in the i-region rapidly increased. This result reveals the significant relationship between the current density in the *I–V* curve and the recombination behaviour. To understand this behaviour in more detail, figure 4(c) presents the band diagrams with their corresponding carrier concentration plots. For simplicity, we plot representative results at selected voltages (0, 1.4, 2.0, 2.4, and 2.54 V; in figure 4(c), the bold solid line and dashed–dotted line indicate the band diagram and the carrier concentration, respectively). The different ranges of bias voltage can be explained by the following mechanism: (i) From 0–1.4 V, the increasing bias voltage gradually decreased the energy band at the p-side (see figures 4(c)), but carriers could effectively escape from the i-region because the built-in fields maintained a strong drift force. Therefore, in this range of bias voltages, negligible recombination occurred and carrier concentration accumulation was minimal; thus, the current density in the *I–V* curve remained almost constant. (ii) In the 1.4–2.0 V range, the energy band in the i-region was extremely flat despite the increased bias voltage. Because carriers can easily recombine in the flattened region, recombination rate was rapidly increased in i-region by increasing the bias voltage; consequently, the current density in the *I–V* curve abruptly decreased over this range of bias voltages. (iii) In the 2.0–2.4 V range, the current density in the *I–V* curve again remained constant as the recombination rate was suppressed in the i-region. The limited recombination rate is probably due to the potential valleys formed at the n- and p-sides (particularly at the p-side) of the InGaN/GaN interface regions because it leads to separate the electron and hole wavefunctions in the i-region, as observed in conventional InGaN/GaN LEDs. Consequently, as the bias voltage increased, carriers began accumulating in the potential valleys rather than recombining in the i-region, and the current density in the *I–V* was scarcely reduced (remained almost constant). The result of Neufeld *et al* [20] was also able to support this explanation. They reported that the current constant region at high bias voltage condition in *I–V* curves became shorter and finally removed by increasing doping density only at n- and p-side InGaN/GaN interface regions, leading to suppress carrier storage by decreasing the potential height. (iv) In the 2.4–2.54 V range, the recombination rate increased with increasing bias voltage because the potential valleys became filled with carriers. Moreover, as most of the built-in field was displaced by the applied bias voltage, diffusion force strengthened with increasing the bias voltage. Consequently, the current density in the *I–V* curve gradually decreased over this range of bias voltage. At 2.54 V, the diffusion force exceeded the drift force and the current density declined to zero. This mechanism confirms that the staircase-like feature arises from the shape of the energy band in the i-region showing the reduced angle of energy band with high height of potential barrier which were affected by piezoelectric fields having opposite direction to built-in fields. For the same reason, current loss occurs in the piezoelectric field structure.

In the above investigations, the In fraction of the p–i–n $In_xGa_{1-x}N$ structure was maintained constant at 0.1. However, to develop a highly efficient $In_xGa_{1-x}N$ SC, the absorption range

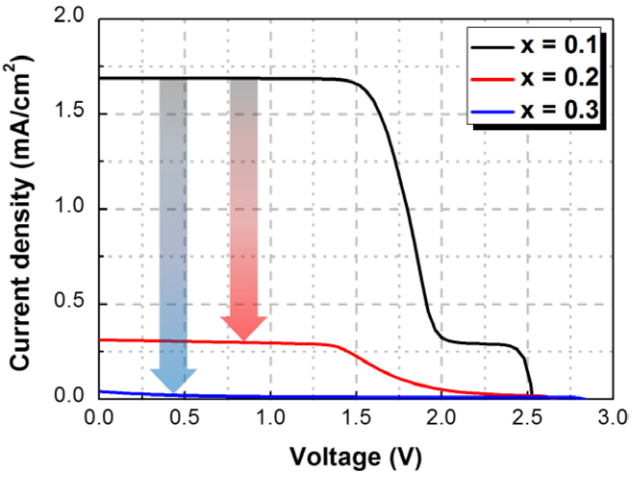

Figure 5. *I–V* characteristics of InGaN SC structures with different In fractions.

Table 2. Simulated device performances of InGaN SC structures with different In fractions.

	In fraction		
	0.1	0.2	0.3
V_{oc} (V)	2.52	2.65	2.84
J_{sc} (mA cm^{-2})	1.69	0.31	0.04
C.E. (%)	1.68	0.26	0.02
F.F. (%)	59.15	46.20	23.45

of incident solar radiation must be increased by increasing the In fraction of the $In_xGa_{1-x}N$ layer. Therefore, we re-simulated the previous SC structure with different In compositions of the i-layer. The *I–V* characteristics and device performances of these structures are presented in figure 5 and table 2, respectively. We observe that the V_{oc} gradually increased as the In-composition increased, whereas the J_{sc} value significantly decreased, although the carrier generation rate was approximately 3 and 7 times larger at the higher In-compositions (the carrier generation rate plots are omitted, but the integrated carrier generation rates in the i-regions of structures with In fractions of 0.1, 0.2, and 0.3 were 8.58×10^{22}, 2.67×10^{23}, and 5.67×10^{23} cm^{-2} s, respectively). These results can be explained by figure 6, which presents the band diagrams, recombination rates, and carrier concentration plots for each structure under 0 V bias. As the In fraction increased, the height of the potential barrier increased in both interface regions as the piezoelectric fields strengthened in the i-region. Subsequent to the increased barrier height, the V_{oc} increased as discussed above. However, the J_{sc} was dramatically decreased at higher In fractions, because the recombination rate in the i-region increased from 3.79×10^{16} to 9.72×10^{21} cm^{-3} s^{-1} as the In fraction varied from 0.1 to 0.3 (figure 5(b)). As expected, this trend in the recombination rate was associated with the shape of the energy band in the i-region. At In fractions of 0.2 and 0.3, the energy band in the i-region was already reverse-tilted before any bias voltage was applied. Therefore, in contrast to the structure with 0.1 In fraction, the recombination process was promoted over carrier escape. Furthermore,

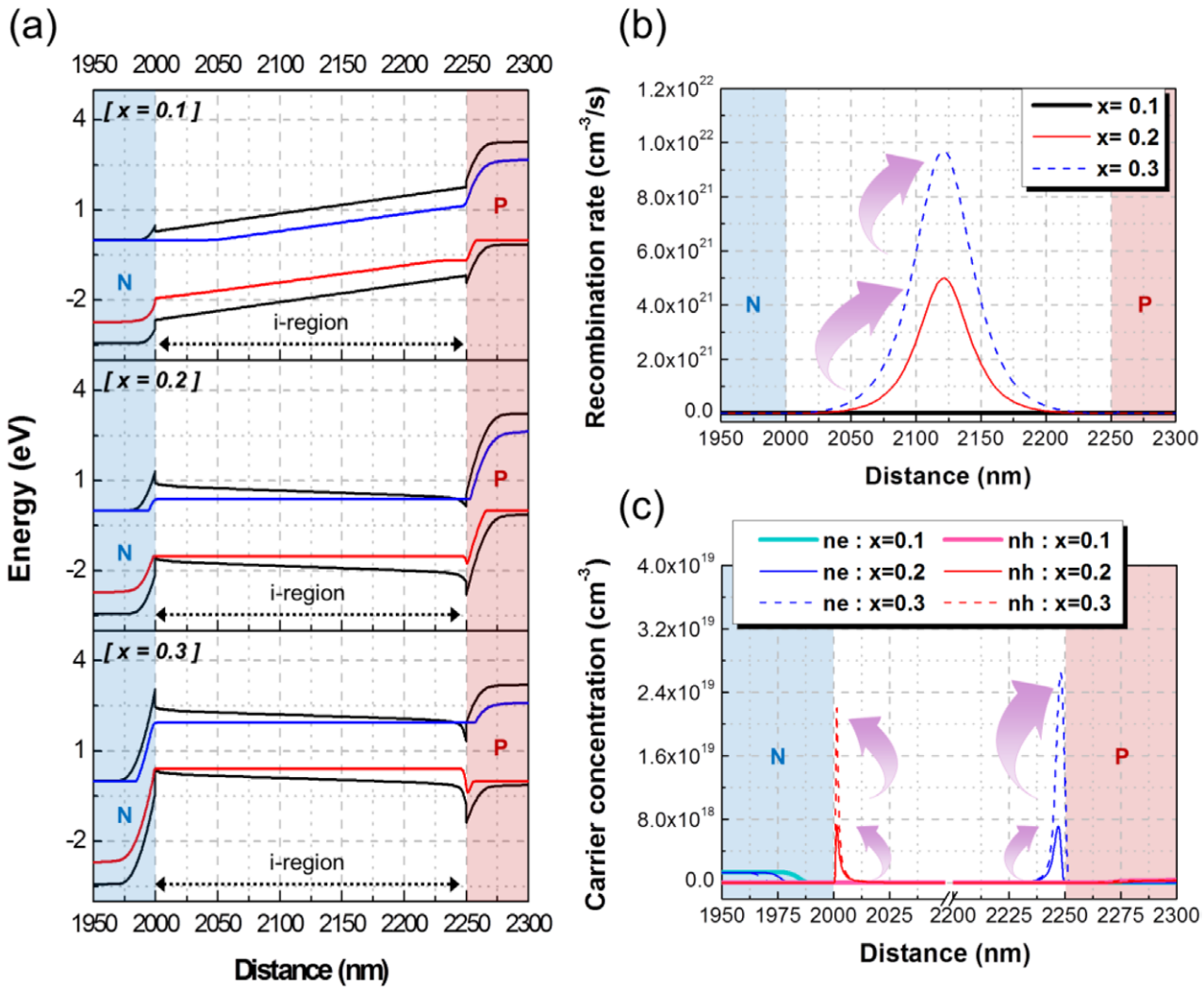

Figure 6. Various characteristics of InGaN SC structures with different In fractions at 0 V: (a)–(c) band diagrams, (b) recombination rates, and (d) carrier concentration plots.

increasing the In fraction deepened the potential valleys by enhancing the opposition of piezoelectric fields to the built-in fields. Consequently, at high In content, carriers became significantly accumulated at both sides of the interface regions (figure 5(c), so that the C.E. and F.F. values decreased as the In-fraction increased, indicating high current loss).

4. Conclusions

This study investigated the effects of piezoelectric fields on the carrier dynamics of InGaN-based solar cell structures. By changing the strain relaxation constants, we confirmed that the piezoelectric fields in the InGaN layer altered the shape of the energy band in the i-region. As the angle of the energy band in the i-region was reduced by the piezoelectric fields, significant current loss occurred in the p–i–n $In_{0.1}Ga_{0.9}N$ SC structure. In particular, the current loss was indicated as a staircase-like feature in *I*–*V*, which was highly related to the recombination process. Despite this loss, the V_{oc} and J_{sc} properties were slightly improved in the structure with piezoelectric fields. In addition, the harmful current loss induced by the piezoelectric fields was amplified at higher In fractions in the InGaN layer. Therefore, to realize high-efficiency solar cells, solutions that eliminate the piezoelectric fields are absolutely required.

Acknowledgment

This work was supported by the NEDO Project.

References

[1] Wu J, Walukiewicz W, Yu K M, Ager J W III, Haller E E, Lu H, Schaff W J, Saito Y and Nanishi Y 2002 *Appl. Phys. Lett.* **80** 3967
[2] Vurgaftman I and Meyer J R 2003 *J. Appl. Phys.* **94** 3675
[3] De Vos A 1992 *Endoreversible Thermodynamics of Solar Energy Conversion* (Oxford: Oxford University Press) p 90
[4] Nanishi Y, Saito Y and Yamaguchi T 2003 *Japan. J. Appl. Phys.* **42** 2549
[5] Jani O, Ferguson I, Honsberg C and Kurtz S 2007 *Appl. Phys. Lett.* **91** 132117
[6] Yong A M, Soh C B, Zhang X H, Chow S Y and Chua S J 2007 *Thin Solid Films* **515** 4496

[7] Soh C B, Chow S Y, Tan L Y, Hartono H, Liu W and Chua S J 2008 *Appl. Phys. Lett.* **93** 173107
[8] Fiorentini V, Bernardini F, Della Sala F, Di Carlo A and Lugli P 1999 *Phys. Rev.* B **60** 8849
[9] Letay G, Hermle M and Dett A W 2006 *Prog. Photovolt. Res. Appl.* **14** 638
[10] Romanov A E, Baker T J, Nakamura S and Speck J S 2006 *J. Appl. Phys.* **100** 023522
[11] Leszcynski M, Suski T, Teisseyre H, Perlin P, Grzegory I, Jun J, Porowski S and Moustakas T D 1994 *J. Appl. Phys.* **76** 4909
[12] Akasaki I and Amano H 1997 *Japan. J. Appl. Phys.* **36** 5393
[13] Ambacher O 1998 *J. Phys. D: Appl. Phys.* **31** 2653
[14] Shimada K, Sota T and Suzuki K 1998 *J. Appl. Phys.* **84** 4951
[15] Morales F M, Gonzalez D, Lozano J G, Garcia R, Hauguth-Frank S, Lebedev V, Cimalla V and Ambacher O 2009 *Acta Mater.* **57** 5681
[16] van Schilfgaarde M, Sher A, Chen A-B 1997 *J. Cryst. Growth* **178** 8
[17] Nakamura S, Pearton S and Fasol G 2013 *The Blue Laser Diode* (Berlin: Springer) p 45
[18] Bernardini F, Fiorentini V and Vanderbilt D 1997 *Phys. Rev.* B **56** R10024
[19] Kuwahara Y, Fujii T, Fujiyama Y, Sugiyama T, Iwaya M, Takeuchi T, Kamiyama S, Akasaki I and Amano H 2010 *Appl. Phys. Express* **3** 111001
[20] Neufeld C F, Cruz S C, Farrell R M, Iza M, Lang J R, Keller S, Nakamura S, DenBaars S P, Speck J S and Mishra U K 2011 *Appl. Phys. Lett.* **98** 243507